Eur. Phys. J. A (2020) 56:165
https://doi.org/10.1140/epja/s10050-020-00167-z

THE EUROPEAN PHYSICAL JOURNAL A

Regular Article - Experimental Physics

Study of excited states and observation of collective level structures in the odd–odd nucleus ^{194}Bi

A. Herzáň[1,2,3,a], S. Juutinen[3], K. Auranen[3], T. Grahn[3], P.T. Greenlees[3], K. Hauschild[3,5], U. Jakobsson[3,6], R. Julin[3], S. Ketelhut[3], M. Leino[3], A. Lopez-Martens[3,5], T. Lönnroth[4], P. Nieminen[3,7], M. Nyman[3,8], J. Partanen[3], P. Peura[3,9], P. Rahkila[3], P. Ruotsalainen[3], M. Sandzelius[3], J. Sarén[3], C. Scholey[3,10], J.M.K. Slotte[4], J. Sorri[3,11], S. Stolze[3,12], J. Uusitalo[3]

[1] Institute of Physics, Slovak Academy of Sciences, SK 84511 Bratislava, Slovakia
[2] Oliver Lodge Laboratory, University of Liverpool, Liverpool L69 7ZE, UK
[3] University of Jyvaskyla, Department of Physics, P.O. Box 35, FI-40014 University of Jyvaskyla, Finland
[4] Physics, Faculty of Science and Engineering, Åbo Akademi University, 20500 Turku, Finland
[5] Present Address: CSNSM, IN2P3-CNRS, 91405 Orsay Campus, France
[6] Present Address: Laboratory of Radiochemistry, Department of Chemistry, University of Helsinki, P.O. Box 55, 00014 Helsinki, Finland
[7] Present Address: Fortum Oyj, Power Division, P.O. Box 100, 00048 Fortum, Finland
[8] Present Address: European Commission, Joint Research Centre, Retieseweg 111, 2440 Geel, Belgium
[9] Present Address: Helsinki Institute of Physics, University of Helsinki, P.O. Box 64, 00014 Helsinki, Finland
[10] Present Address: MTC Limited, Ansty Park, Coventry CV7 9JU, UK
[11] Present Address: Radiation and Nuclear Safety Authority-STUK, Laippatie 4, 00880 Helsinki, Finland
[12] Present Address: Argonne National Laboratory, 9700 Cass Ave, Lemont, IL 60439, USA

Received: 12 March 2020 / Accepted: 17 May 2020 / Published online: 10 June 2020

Communicated by Robert Janssen

Abstract High-spin states of the odd–odd ^{194}Bi nucleus have been studied by means of nuclear spectroscopy for the first time. Two low-lying rotational bands were observed. The positive-parity band built on a short-lived isomeric state 633 keV above the α and β decaying long-lived (10^-) state is assigned a $\pi i_{13/2} \otimes \nu i^{-1}_{13/2}$ configuration, while the other band is attributed to the $\pi h_{9/2} \otimes \nu i^{-1}_{13/2}$ configuration. Both of these bands are assumed to have oblate shape. Three band-like structures composed predominantly of $\Delta I = 1$ transitions were also found. One of the shears band candidates is firmly linked to the lower lying level structures whereas for the other two links to lower-lying structures remain missing.

1 Introduction

Nuclear structure studies of the odd–odd nuclei are generally rather challenging due to high level density available for the valence nucleons, hence, their excitation level schemes are usually more complicated than in neighbouring even–even and odd-mass nuclei. At the same time, the established level schemes provide essential information of nuclear structure, like residual proton–neutron interaction, odd–even staggering and signature inversion in rotational bands etc. [1] when nuclei are stressed by the high spin. These phenomena and related topics are the main reason for systematic studies of the deformed odd–odd heavy nuclei in which 2-quasiparticle (qp) and 4-qp rotational structures can exist. Recently, we have studied the Z = 83 isotopes ^{193}Bi and ^{195}Bi [2,3]. The obtained level schemes are good examples of shape co-existence. The appearance of collectivity is related to the 2p–2h excitations across the Z = 82 shell gap. According to the TRS calculations for ^{193}Bi [4], the proton $i_{13/2}$ $13/2^+[606]$ and $7/2^-[514]$ of mixed $f_{7/2}/h_{9/2}$ configurations favour oblate shapes with $\beta_2 \approx 0.21$ and 0.19, respectively. Similarly in ^{194}Bi, collective level structures are expected for the configurations which involve these proton orbitals.

In the early 1990s, several groups independently proposed an evidence for the experimental discovery of a new type of rotational excitations in the light-Pb isotopes [5–8]. The corresponding rotational-like structures composed of sequences of magnetic dipole transitions were associated with nearly spherical shape of nucleus. Existence of such structures with so low quadrupole deformation caused a puzzle. It was theoretically addressed by means of the tilted axis cranking

T. Lönnroth, J. Partanen: Deceased.

[a] e-mail: andrej.herzan@savba.sk (corresponding author)

model, and a new type of nuclear excitation – *shears mechanism* was introduced [9]. The competition between the shears mechanism and core rotation in the framework of a classical solution of a particles-plus-rotor model was presented in Ref. [10]. Magnetic rotation, or shears bands, have also been experimentally and theoretically studied in other mass regions, see *e.g.* Refs. [11–19]. In addition, information on magnetic rotation in the very neutron-deficient Bi isotopes is scarce. Rare finding of a crossing of two shears bands associated with multi-quasiparticle configurations was reported for the ^{198}Bi nucleus [20]. In the odd-A ^{197}Bi nucleus, Mabala *et al.* [21] suggested that the larger values of $\Im^{(2)}$ for a shears band are a result of the involvement of the intruder proton $i_{13/2}$ orbital. A configuration with three high-K protons, $\pi(h^2_{9/2}i_{13/2})_{K=14.5}$, was proposed. This is very different from dynamic moments of inertia and configurations involving one high-K $h_{9/2}$ proton for shears bands in heavier Bi isotopes [22]. On the other hand, a five-qp configuration with three high-K protons, $\pi(h^2_{9/2}i_{13/2}) \otimes \nu(i^{-1}_{13/2}p^{-1}_{3/2})$, was also proposed for a shears band in ^{195}Bi [3]. So far, no shears band is reported for ^{196}Bi. Existence of shears bands in lighter odd–odd Bi isotopes associated with multi-qp configurations is anticipated.

In the neutron-deficient odd–odd nuclei around lead, two α-decaying isomeric states are known [23–31]. On the basis of the feeding pattern in the β^+/EC decay, systematics, and the observation of unhindered α decay to ^{190}Tl, the (10^-) and (3^+) spin and parity assignments of these two isomers in ^{194}Bi were made [29,30]. These isomeric states are associated with the $\pi h_{9/2} \otimes \nu i^{-1}_{13/2}$ and $\pi h_{9/2} \otimes \nu p_{3/2}$ configurations, respectively.

Based on the mass measurement of ^{190}Tl and the subsequent exploitation of the α-decay energies, excitation energy of the (10^-) isomeric state has been calculated to be 184(12) keV [32]. Recent measurement of the α-decay properties of ^{202}Fr [33] places the (10^-) isomeric state to an excitation energy of 161(8) keV based on α-γ coincidences.

In Ref. [30], two coincident γ-ray transitions with energies of 181 keV and 218 keV were tentatively placed to feed the (3^+) ground state in ^{194}Bi. The α-decay study of ^{202}Fr [33] confirmed the placement of the two transitions, and at the same time extended the knowledge of the ^{194}Bi nucleus by providing the energies of the three transitions feeding the (10^-) isomeric state. Information about higher spin states was not available until the present study. In the neighbouring odd–odd ^{196}Bi nucleus, the information on excited states is also limited. Although a superdeformed (SD) band has been reported in Ref. [34], the decay scheme for low-lying states in ^{196}Bi is limited to two γ-ray transitions depopulating the isomeric states [35]. The isomeric (10^-) state decays via the 102 keV E3 transition to the $|\pi h_{9/2} \otimes \nu f_{5/2}; 7^+\rangle$ state. In ^{194}Bi, this state is expected at higher energy, since the $f_{5/2}$ orbital moves further away from the Fermi surface with decreasing neutron number. In-beam studies of ^{198}Bi have revealed both non-collective states and magnetic-rotation (MR) bands [20,36,37].

In this work, we report on the results of the first spectroscopic study of excited states above the (10^-) isomeric state in ^{194}Bi. The JUROGAM II + RITU + GREAT setup was used. In total, five bandlike structures were observed, while three of them may be associated with magnetic rotation. Due to long half-lives and small branching ratios, the α decays of the ^{194}Bi nucleus could not be studied.

2 Experimental details

The experiment was carried out at the Accelerator Laboratory of the University of Jyväskylä (JYFL), Finland. The fusion-evaporation reaction ^{159}Tb(^{40}Ar,5n) was used to produce ^{194}Bi nuclei. The experiment itself had two phases:

(i) A JUROGAM II standalone experiment employing a backed target comprising of ^{159}Tb with thickness of 1.2 mg cm^{-2} (Au backing). The target was bombarded with an ^{40}Ar beam, accelerated by $K = 130$ MeV cyclotron to an energy of 182 MeV. The average beam intensity was 3 particle nA (pnA).
(ii) A JUROGAM II + RITU experiment employing a thin ^{159}Tb target, with thickness of 320 μg cm^{-2} supported by a C foil was bombarded with 190 MeV ^{40}Ar beam. For the purpose of an excitation function measurement, a short run with a beam energy of 185 MeV was also performed. In this phase the beam intensity was increased to 9 pnA.

Prompt γ rays were measured by utilising the fully digitised JUROGAM II High-Purity Germanium (HPGe)-detector array. The recoil separator RITU [38,39] was used to clean the recoiling fusion-evaporation products from unwanted particles, and focused them to the focal plane GREAT spectrometer [40] which was housing a planar Ge detector, and surrounded by three clover-type HPGe detectors. In the GREAT spectrometer, characterisation of the implanted particles was performed. More details on the configuration and all settings of the experimental setup is given in Ref. [3].

The data, recorded synchronously using the triggerless total data readout (TDR) [41] data acquisition system, were processed using the GRAIN [42] and RADWARE [43,44] software packages.

3 Results

The ^{194}Bi nucleus is known to have two α-decaying isomeric states [30]. The (3^+) state, which is assumed to be the ground

state [$E_\alpha = 5645(5)$ keV, a total $b_\alpha = 0.46(25)$ %, $T_{1/2} = 95(3)$ s] and the (10^-) isomeric state [$E_\alpha = 5599(5)$ keV, $b_\alpha = 0.20(7)$ % and $T_{1/2} = 115(4)$ s] [30]. Small α-decay branches and long half-lives do not allow for a reasonable recoil-decay tagging (RDT) analysis [45]. Hence, the analysis relies on the recoil gating technique.

In our data analysis, both the thin and backed target data sets were used. A large number of new states have been found. The related γ-ray transitions are listed in Table 1, together with their multipolarities. In order to establish the ordering of the transitions, γ-γ coincidence matrices and γ-γ-γ cubes were generated and analysed. The resulting level scheme is presented in Fig. 1. All the observed level structures are placed to feed the (10^-) isomeric state. Delayed γ rays were searched for at the focal plane up to 50 μs after recoil implantation in the DSSD. We found no delayed γ-ray transitions associated with ^{194}Bi.

The DCO (directional correlations deexciting oriented states [46]) and IPDCO (integrated polarizational-directional correlation from oriented nuclei [47]) analyses were performed. Experimental angular distribution ratios (R_{expt}) and linear polarisation asymmetry factors (A_P) were extracted from JUROGAM II data in similar fashion as in Ref. [2]. In this work, typical R_{expt} values for stretched dipole and quadrupole transitions are 0.7 and 1.2, respectively. Average values of A_P are -0.12 and $+0.12$ for transitions with magnetic and electric characters, respectively. The values of R_{expt} and A_P are as well listed in Table 1.

The first in-beam γ-ray spectroscopy study of ^{194}Bi is presented. Analysis of JUROGAM II γ-γ coincidences revealed five different cascades of transitions in total that can be treated as rotational bands. Two of them are found to be regular strongly coupled rotational bands. The remaining three bands resemble magnetic rotation.

3.1 Strongly coupled bands

3.1.1 Band 1

Strongly coupled rotational Band 1 is the most intensely populated level structure in this experiment. In Fig. 2a, the spectrum of prompt γ rays gated on the 227 keV transition is shown. Transitions corresponding to Band 1 are clearly visible. In our study, we observe Band 1 up to a spin and parity of $I^\pi = (18^+)$ and an excitation energy of 2931 keV above the (10^-) isomeric state. Based on the comparisons with ^{193}Bi and ^{195}Bi, we associate this band with the $\pi i_{13/2} \otimes \nu i^{-1}_{13/2}$ configuration, and hence with positive parity.

Main decay out of Band 1 proceeds via emission of the 633 keV γ ray. It is the strongest γ ray in the singles prompt γ-ray spectrum. Second decay branch depopulates the 794 keV level via the combination of the 105 and 529 keV transitions down to the (10^-) isomeric state, see Fig. 1. The 105 keV γ-ray peak appears small in the gated γ-ray spectra. On the contrary, the 529 keV γ-ray peak is clearly visible in Fig. 2a. Spectrum of prompt γ rays gated on the 529 keV transition, as presented in Fig. 2b, shows no sign of the 633 keV transition. However the 105 keV transition, together with Band 1 members, is now clearly present in the spectrum. The two parallel decay branches of Band 1 are also confirmed by the analysis of triple-γ coincidences.

The recoil shadow anisotropy method (RSAM) [48] that we applied to our JUROGAM II data indicates the 794 keV level to have an isomeric character. Rather consistent anisotropies, A_γ (%): 6.20, 8.20, 6.40 for the 105, 529 and 633 keV γ rays, in combination with recoil velocity $v/c \approx 2.0$ % yields half-life of $T_{1/2} \approx 1$ ns. The nanosecond half-life disturbs measured DCO ratios, R_{expt}, and linear polarisation asymmetry factors, A_P, in the thin target data. From the backed target data, we get $R_{expt}(529\,\text{keV}) = 0.72(7)$ ($\Delta I = 1$) and $R_{expt}(633\,\text{keV}) = 1.43(11)$. The latter value is consistent with the $\Delta I = 0$ dipole transition. Therefore, we assign the band head of Band 1 with $I^\pi = (10^+)$.

Multipolarities of the 105 and 529 keV transitions, respectively, can be deduced from the intensity balance analysis: (i) Total transition intensities corrected for the JUROGAM II detection efficiency $I_{tot}(105\,\text{keV}, M1) = 13.8(21)$ {$\alpha_{th} = 8.96(13)$ [49]} and $I_{tot}(529\,\text{keV}, E1) = 12.5(8)$. (ii) $I_{tot}(105\,\text{keV}, E1) = 1.96(29)$ and $I_{tot}(529\,\text{keV}, M1) = 13.6(9)$. Hence, the 105 and 529 keV transitions are assigned with $M1$ and $E1$ character, respectively. The γ-γ coincidences are not helpful in fixing the ordering of these two transitions in the level scheme. If the 105 keV M1 transition is placed to depopulate the 794 keV level, the resultant 689 keV level should have either $I^\pi = (9^+)$ or (11^+). Furthermore, the reduced transition rate for the 105 keV transition would be $\approx 10^{-5}$ W.u., indicating very different configurations for the 689 and 794 keV levels. However, the $\pi i_{13/2} \otimes \nu i^{-1}_{13/2}$ configuration is the only 1p-1n configuration available for such spin values. Instead, when the 529 keV transition is placed to depopulate the 794 keV level, the 266 keV level has either $I^\pi = (9^-)$ or (11^-). The lower spin alternative is adopted in Fig. 1, since no side feeding is observed to the 266 keV level. In fact, the 105 keV transition can be identified to be a member of the same $p-n$ multiplet as the isomeric (10^-) state (more details in section 4.3). Placement of the 105 keV transition in our level scheme (see Fig. 1) is also confirmed by the $\alpha-\gamma$ coincidence measurement in Ref. [33].

A group of transitions labeled as Group A is placed on the left of Band 1 in our level scheme, see Fig. 1. Many other transitions belonging to this level structure are listed in Table 1. Positive parity is assigned to majority of levels in Group A as they are found to de-excite to the members of positive parity Band 1.

Table 1 Energies E_γ, relative intensities (obtained from JUROGAM II data) I_γ, excitation energies E_i, and initial and final spins I_i^π and I_f^π, respectively, for the γ-ray transitions assigned to ^{194}Bi. Also angular distribution ratios R_{expt}, linear polarisation asymmetry factors A_P, and multipolarities are shown. D in the multipolarity column denotes a stretched dipole transition. The intensities have been normalised with respect to the 227 keV $(12^+) \rightarrow (11^+)$ transition. The systematic error of about 0.3 keV should be added to the fitting errors given for most of the transitions listed in the first column

E_γ (keV)	I_γ (%)	E_i (keV)	I_i^π	I_f^π	R_{expt}	A_P	Multipolarity
Band 1							
104.6(1)[1]	5.3(3)	266	(9^-)	(10^-)			$M1$
142.3(1)	50.9(16)	936	(11^+)	(10^+)	0.60(5)		$M1$
227.0(1)	100(3)	1163	(12^+)	(11^+)	0.61(5)		$M1$
263.4(1)	75.7(23)	1427	(13^+)	(12^+)	0.61(5)		$M1$
294.0(1)	61.8(19)	1721	(14^+)	(13^+)	0.71(5)	-0.051(4)	$M1$
313.2(1)	43.1(13)	2034	(15^+)	(14^+)	0.66(5)	-0.074(5)	$M1$
334.6(1)	18.2(6)	2368	(16^+)	(15^+)	0.79(7)	-0.18(2)	$M1$
353.3(1)	5.1(3)	2721	(17^+)	(16^+)	0.86(9)		$M1$
368.8(2)	5.1(14)	1163	(12^+)	(10^+)			$E2$
371.3(1)	4.1(3)	3092	(18^+)	(17^+)			$M1$
490.3(1)	11.1(5)	1427	(13^+)	(11^+)	1.12(11)		$E2$
528.6(1)[1]	37.6(13)	794	(10^+)	(9^-)	0.72(7)		$E1$
557.3(1)	15.0(6)	1721	(14^+)	(12^+)	1.26(11)	0.060(6)	$E2$
606.9(1)	15.5(6)	2034	(15^+)	(13^+)	1.24(10)	0.23(2)	$E2$
633.1(1)[1]	247(8)	794	(10^+)	(10^-)	1.43(11)		$E1$
647.4(1)	8.4(4)	2368	(16^+)	(14^+)	1.14(10)	0.22(3)	$E2$
688.2(2)	3.3(2)	2721	(17^+)	(15^+)	1.19(14)		$E2$
723.7(1)	3.0(2)	3092	(18^+)	(16^+)	2.1(3)		$E2$
Band 2							
107.9(1)	1.9(2)	1018					
243.3(1)	17.5(6)	1592	(14^-)	(13^-)	0.80(7)	-0.18(2)	$M1$
289.9(1)	5.3(3)	2245	(16^-)	(15^-)			$M1$
330.2(1)	33.1(12)	1349	(13^-)	(12^-)	0.59(6)	-0.086(7)	$M1$
331.3(1)	15.2(6)	1018	(12^-)	(11^-)			$M1$
363.4(1)	15.5(6)	1955	(15^-)	(14^-)	0.68(7)	-0.109(10)	$M1$
400.9(1)	4.5(4)	2646	(17^-)	(16^-)			$(M1)$
437.7(1)	3.7(3)	1349	(13^-)	(11^-)			
526.2(1)	>68	687	(11^-)	(10^-)	0.53(7)	-0.020(2)	$M1$
573.6(1)	27.8(12)	1592	(14^-)	(12^-)	1.19(14)	0.018(2)	$E2$
606.6(1)	12.5(7)	1955	(15^-)	(13^-)	1.20(12)		$E2$
653.5(1)	14.4(6)	2245	(16^-)	(14^-)	1.30(13)	0.064(8)	$E2$
661.8(1)	16.2(6)	1349	(13^-)	(11^-)	1.10(13)	0.15(3)	$E2$
690.8(1)	7.2(3)	2646	(17^-)	(15^-)			$(E2)$
733.1(1)	4.2(3)	2978	(18^-)	(16^-)	1.04(14)		$(E2)$
857.5(1)	59(3)	1018	(12^-)	(10^-)	1.37(13)	0.050(4)	$E2$
Band 3							
(59.6(1))	2.8(2)	2428	(16^+)	(16^+)			$M1$
184.5(1)	10.5(4)	2613	(17^+)	(16^+)	0.78(8)		$M1$
354.5(1)	14.7(5)	2967	(18^+)	(17^+)	0.42(8)		$M1$
394.2(1)	23.6(8)	2428	(16^+)	(15^+)	0.77(9)	-0.07(4)	$M1$
433.2(1)	3.3(2)	3844		(19^+)			
444.2(1)	8.2(3)	3411	(19^+)	(18^+)	0.98(13)		$M1$

Table 1 continued

E_γ (keV)	I_γ (%)	E_i (keV)	I_i^π	I_f^π	R_{expt}	A_P	Multipolarity
457.9(2)	1.9(2)	4302					
707.3(1)	16.9(6)	2428	(16^+)	(14^+)	1.2(2)	0.13(5)	$E2$
Band 4							
139.4(1)[2]	>9.6	$x+139$	(18)	(17)	0.67(8)		$(M1)$
141.3(1)[2]	9.6(8)	$x+281$	(19)	(18)	0.67(8)		$(M1)$
165.9(1)	9.1(5)	$x+447$	(20)	(19)	0.87(10)		$(M1)$
201.7(1)	9.1(4)	$x+648$	(21)	(20)	0.68(8)	-0.18(4)	$M1$
242.7(1)	10.5(4)	$x+891$	(22)	(21)	0.67(10)	-0.063(7)	$M1$
267.3(1)	2.3(2)	$x+2670$	(28)	(27)			$(M1)$
274.8(1)	8.1(3)	$x+1166$	(23)	(22)	0.69(8)	-0.13(3)	$M1$
285.8(1)	3.8(2)	$x+2403$	(27)	(26)			$M1$
303.2(1)	8.4(4)	$x+1469$	(24)	(23)	0.62(8)		$(M1)$
318.0(1)	5.1(2)	$x+2117$	(26)	(25)			$(M1)$
330.3(1)	6.5(3)	$x+1799$	(25)	(24)	0.8(8)		$M1$
444.1(3)	1.8(3)	$x+891$	(22)	(20)			$(E2)$
517.9(2)	2.1(2)	$x+1166$	(23)	(21)			$(E2)$
577.6(3)	2.0(2)	$x+1469$	(24)	(22)			$(E2)$
Band 5							
124.8(1)	>20.4	$y+125$	(i+1)	i	0.59(6)		$(M1)$
211.1(1)	16.3(10)	$y+336$	(i+2)	(i+1)	0.65(6)	-0.13(4)	$M1$
259.2(1)	13.4(6)	$y+595$	(i+3)	(i+2)	0.83(7)		$(M1)$
363.4(1)	4.8(3)	$y+958$	(i+4)	(i+3)	0.78(11)		$(M1)$
438.1(1)	2.6(2)	$y+1397$	(i+5)	(i+4)	0.76(8)		$(M1)$
Group A							
153.2(1)	5.1(3)	1316	(11^+)	(12^+)			$M1$
183.9(1)	8.9(4)	1500	(12^+)	(11^+)	0.69(12)	-0.12(2)	$M1$
(347.9(2))	1.7(2)	2808		(16)			
379.7(1)	9.1(5)	1316	(11^+)	(11^+)	1.7(2)		$M1$
427.0(1)	5.6(3)	2461	(16)	(15^+)	0.83(10)		D
456.7(1)	10.3(5)	1957		(12^+)		-0.17(3)	$(M1)$
485.4(1)	6.2(3)	1985		(12^+)			
560.4(1)	8.4(4)	2060		(12^+)			
564.4(1)	6.7(4)	1500	(12^+)	(11^+)			$M1$
576.0(1)	10.0(7)	1370		(10^+)		-0.12(2)	$(M1)$
705.3(1)	8.2(6)	1500	(12^+)	(10^+)	1.4(3)	0.16(2)	$E2$
750.4(1)	4.6(3)	2784		(15^+)	1.06(12)		$(M1+E2)$
842.6(1)	5.8(4)	2269		(13^+)		-0.076(6)	$(M1)$
Group B							
283.1(2)	1.6(2)	1926		(13^-)			
587.7(3)	2.0(3)	2230	(15^-)	(13^-)			$(E2)$
604.8(2)	2.3(3)	2087		(12)			
624.5(4)	2.5(5)	1643	(13^-)	(12^-)			$(M1)$
670.4(2)	3.6(3)	1896	(13^-)	(12^-)	0.8(3)		$M1$
695.3(1)	6.7(4)	1382	(11^-)	(11^-)	1.4(2)		$(M1)$
706.1(1)	8.1(6)	1725		(12^-)			
738.1(1)	5.2(3)	2087		(13^-)		-0.18(5)	$M1$

Table 1 continued

E_γ (keV)	I_γ (%)	E_i (keV)	I_i^π	I_f^π	R_{expt}	A_P	Multipolarity
795.1(1)	9.7(5)	1482	(12)	(11^-)	0.60(8)		D
881.7(2)	3.0(3)	2230	(15^-)	(13^-)	1.1(2)	0.16(4)	$E2$
956.0(1)	9.8(5)	1643	(13^-)	(11^-)	0.94(11)	0.16(3)	$E2$
1157.7(2)	2.7(3)	1845		(11^-)			
1208.6(2)	2.9(3)	1896	(13^-)	(11^-)			$E2$
Group C							
224.6(1)	3.4(2)	2113	(15)	(14^-)	0.85(13)		D
318.2(2)	2.2(2)	2349	(15)	(14^-)			
331.5(1)	4.0(3)	2030	(14^-)	(13^-)			$M1$
472.8(1)	7.0(4)	1699	(13^-)	(12^-)	0.60(9)	-0.04(1)	$M1$
(527.6(1))	4.7(3)	2558		(14^-)			
539.5(1)	8.5(4)	1888	(14^-)	(13^-)	0.87(9)	-0.13(2)	$M1$
541.0(1)	7.0(3)	2429	(16^-)	(14^-)	1.1(2)	0.029(5)	$E2$
662.8(1)	9.7(4)	1888	(14^-)	(12^-)	1.01(13)	0.14(4)	$E2$
681.2(2)	5.2(4)	1699	(13^-)	(12^-)			$M1$
756.7(1)	4.6(3)	2349	(15)	(14^-)	0.68(9)		
804.7(2)	3.2(3)	2030	(14^-)	(12^-)	1.4(3)	0.09(3)	$E2$
1011.4(1)	5.0(3)	1699	(13^-)	(11^-)			$E2$
1064.6(1)	>24	1226	(12^-)	(10^-)	1.26(14)	0.21(4)	$E2$
Group D							
211.0(1)	2.3(2)	911	(11^-)	(10^-)			
539.4(1)	>2.3	700	(10^-)	(10^-)			
749.6(1)	5.7(5)	911	(11^-)	(10^-)			
Other transitions							
131.0(1)[3]	8.2(4)						
158.0(2)[4]	8.2(4)						
162.4(2)[3]	5.5(4)						
184.0(2)[4]	8.2(4)						
205.0(2)[3]	3.7(4)						
237.6(1)[3]	10.9(6)						
241.0(5)[3]	5.0(5)						
249.6(2)[3]	2.0(2)						
289.2(2)[3]	12.6(8)						
304.0(4)[3]	11.1(7)						
325.3(2)[3]	6.2(6)						
437.1(2)[5]							
776.4(1)[6]	2.7(2)	3204		(16^+)			

[1] Transitions below the short-lived (10^+) isomeric state
[2] R_{expt} coefficients cannot be extracted for the two transitions separately in this study
[3] γ-ray transition seen in prompt coincidence with the transitions depopulating the lowest lying states in Band 1 and Group A
[4] γ-ray transition seen in prompt coincidence with transitions of Group C
[5] γ-ray transition seen in prompt coincidence with the 526 and 529 keV transitions from Bands 1 and 2, respectively
[6] A transition feeding the (16^+) band-head state of Band 3

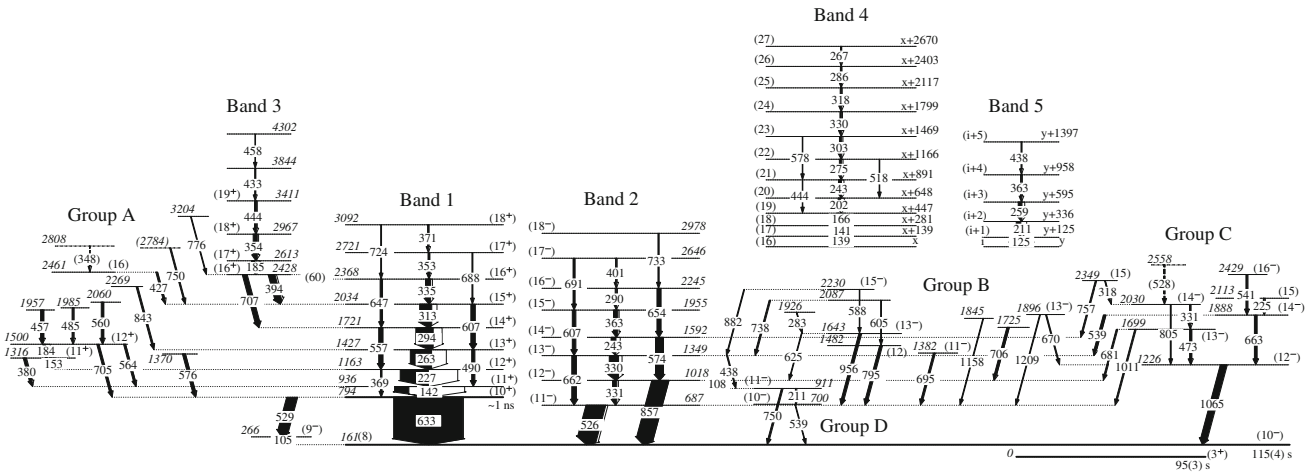

Fig. 1 The level scheme of ^{194}Bi. Widths of the arrows are proportional to the intensities of the transitions in JUROGAM II data. In the level scheme, an excitation energy of the (10^-) isomeric state is taken from Ref. [33]. Among other quantities, also half-lives of the (3^+), (10^-) [30], and the (10^+) (from this study) isomeric states are indicated

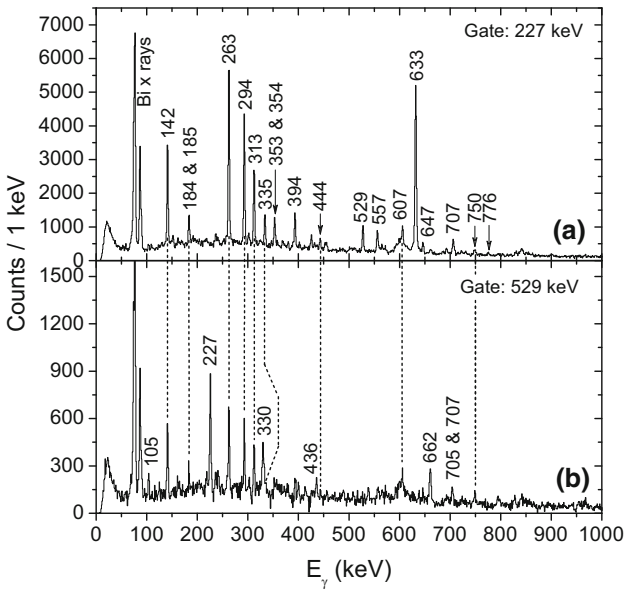

Fig. 2 Measured spectra of prompt γ rays, gated on the (a) 227 keV, and (b) 529 keV transitions, respectively, and mainly associated with Band 1

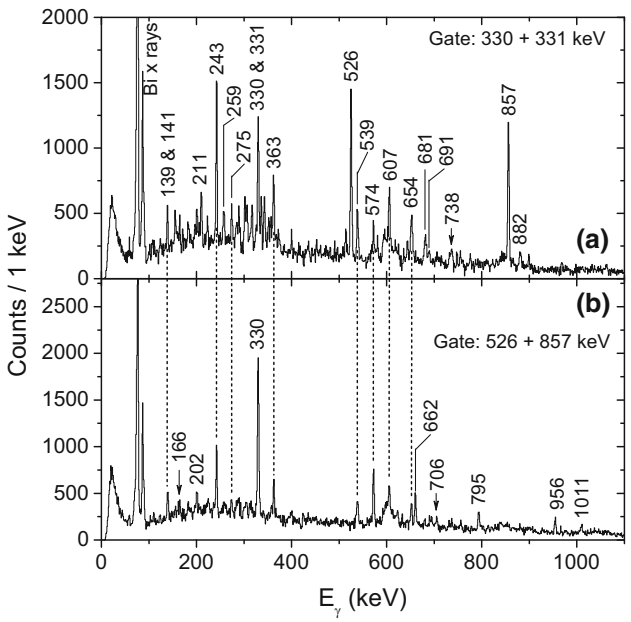

Fig. 3 Spectra of γ rays measured in JUROGAM II and sum gated on the (a) 330 + 331 keV, and (b) 526 + 857 keV transitions, respectively. Labeled peaks correspond to transitions between negative-parity states shown in Fig. 1

3.1.2 Band 2

Inspection of prompt γ-γ coincidence matrix identifies a set of transitions, which form the strongly coupled rotational band (Band 2 in Fig. 1). A γ-ray spectrum gated on the 330 and 331 keV doublet is shown in Fig. 3a. Transitions that form Band 2 are among the strongest in this spectrum. Even though the 526 keV and 529 transitions are part of a doublet in singles γ-ray spectra, the γ-ray peak at 526 keV, relevant for Band 2 analysis, is separated in the gated spectrum shown in Fig. 3a. Such a result is crucial in our analysis, since the 526 keV transition is found to depopulate the lowest observed state of Band 2 to the (10^-) isomeric state. Values of R_{expt} and A_P suggest a stretched $M1$ character for the 526 keV transition. The multipolarity assignment dictates this state to have a spin and parity of $I^\pi = (11^-)$. In Ref. [33], a transition with an energy of 525.4 keV is placed to feed the (10^-) isomeric state. The decay of Band 2 is firmly established by observation of another transition with an energy of 857 keV. It depopulates the (12^-) member of Band 2 (see Fig. 1 and

Table 1). Extra decay path from the $I = (12), (13)$ levels to a different level structure labeled as Group D is observed. The excited state at 911 keV is found to play an important role in the decay out of the strongly coupled Band 2. This will be discussed more in detail later in Section 4. In the present study, the topmost state in Band 2 has $I^{\pi} = (18^{-})$ and is located at 2818 keV above the (10^{-}) isomeric state.

3.2 Groups B and C

In Fig. 3b, a spectrum of γ rays gated on the 526 and 857 keV transitions in the prompt γ-γ matrix is shown. Several new γ-ray peaks can be recognised in this spectrum. None of them belong to aforementioned strongly coupled rotational bands. In the level scheme in Fig. 1, we place these new transitions to form level structures labeled as Groups B and C. Almost entire intensity of the two groups seems to flow to Band 2. However, Group C is also found to directly feed the (10^{-}) isomeric state via the 1065 keV $E2$ transition. It places the yrare (12^{-}) state at an energy of 1226 keV in the level scheme. Based on the DCO and IPDCO analyses, the majority of levels in these groups are assigned a negative parity.

3.3 Dipole bands

Three bandlike structures consisting of intense magnetic dipole transitions, labeled as Bands 3−5, were established in ^{194}Bi. Ordering of the transitions above the spin of $I = (25)$ in Band 4 remains only tentative.

Among these three bands, Band 3 is the only one for which the links to lower-lying structures have been established in this study. Altogether three linking transitions are observed. The band-head spin and parity of $I^{\pi} = (16^{+})$ is firmly given by observing the stretched 394 keV $M1$ and 707 keV $E2$ transitions, depopulating the band head of Band 3 to the (15^{+}) and (14^{+}) members of Band 1. These two transitions, together with a few Band 3 members are visible in the spectra gated on the Band 1 transitions, as shown in Fig. 2. The 60 keV transition is also placed to depopulate Band 3 to Band 1 in the level scheme (see Fig. 1). It is necessary for explanation of coincidence relation between the 335 keV transition and the members of Band 3. From the measured R_{expt} values and intensity balance analysis, we conclude that the lowest-lying member with an energy of 185 keV is an $M1$ transition.

Band 3 is irregular in terms of ordering and energy differences of the transitions. In the present study, Band 3 has been populated up to an excitation energy of 4302 keV. Spins and parities of the two topmost states remain unassigned.

Figure 4 shows transitions relevant for the rotational structure labeled as Band 4 in our level scheme.

We also identified three cross-over transitions with energies of 444, 518 and 578 keV in the gated spectra. Low γ-ray

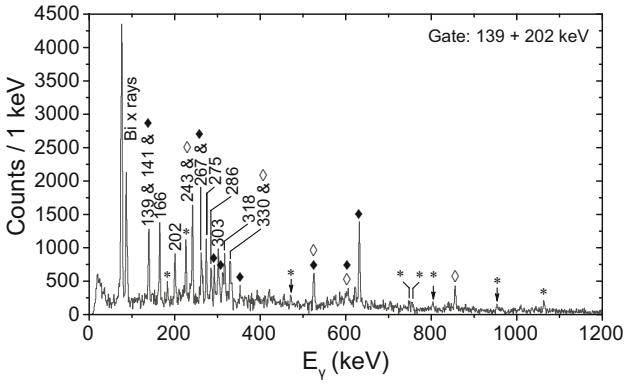

Fig. 4 Prompt γ-ray spectrum gated on the 139 and 202 keV transitions. Peaks with energy label denote members of Band 4. Full and empty diamonds indicate Band 1 and Band 2 members, respectively, and asterisk is for other transitions in ^{194}Bi

intensities and contamination from stronger transitions in the ^{194}Bi level scheme prevent their multipolarities to be determined. A very likely 633 keV $E2$ cross-over transition is not placed in the level scheme due to a presence of the strong 633 keV transition depopulating the yrast (10^{+}) state. The occurrence of cross-over transitions helps with ordering of the transitions in Band 4 to some extent. As evident from Fig. 4, Band 4 de-excites to several lower-lying structures, most notably to Bands 1, 2 and Group C. Several transitions, which belong to Band 4 are also present in Fig. 3. However, linking transitions were not identified.

A sequence of five γ-ray transitions with confirmed stretched dipole multipolarity is labeled as Band 5 in Fig. 1. As a pure magnetic dipole character is assigned to the 211 keV γ-ray transition in Band 5 (see Table 1), and the transition energies within the band smoothly increase, all members are assigned with stretched $M1$ character. The gated γ-ray spectra suggest an isomeric character for the lowest energy level in Band 5, since no transitions from the lower-lying structures are present in the spectra gated on the members of this band. The assignment to ^{194}Bi is confirmed by observation of Bi X rays, and the fact that this sequence has not been observed in neighbouring odd-A Bi nuclei [2,3].

4 Discussion

Considering the previous studies of very neutron-deficient Bi nuclei [2–4,21,50–54], a mixture of spherical and moderately-oblate deformed low-lying structures can be anticipated in ^{194}Bi. The (10^{-}) isomeric state in ^{194}Bi can be interpreted as a member of the two quasiparticle (qp) $|\pi h_{9/2} \otimes \nu i^{-1}_{13/2}; J\rangle$ multiplet, same as in its heavier counterparts. The highest-spin member of this multiplet has $I^{\pi} = (11^{-})$. Therefore, the interpretation of the higher-lying states in ^{194}Bi can be obtained by the coupling of the $h_{9/2}$ proton with the high-

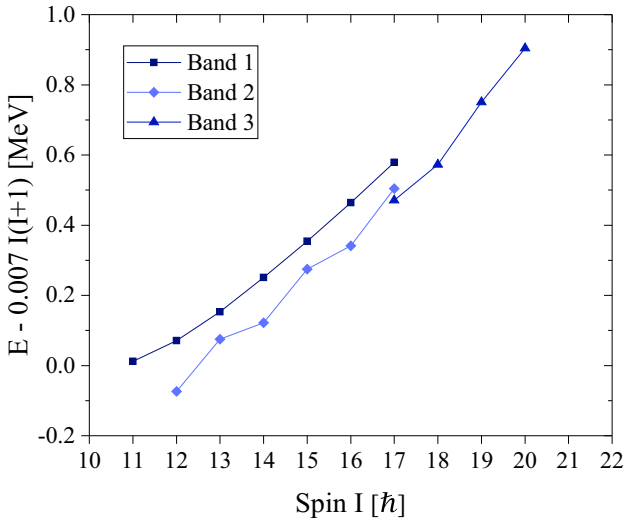

Fig. 5 (Colour online) Excitation energy minus a rigid-rotor reference term, $E(I) - aI(I+1)$ with $a = 0.007 MeV/\hbar^2$, as a function of the spin I illustrates the evolution of the rotational structures with spin in ^{194}Bi, and highlights the spin region where the structure of the yrast line changes

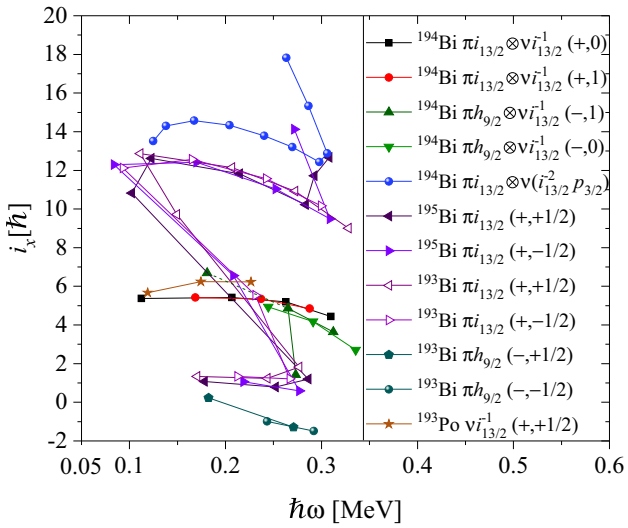

Fig. 6 (Colour online) Aligned angular momenta i_x for the favoured ($\alpha = 0$) and unfavoured ($\alpha = 1$) signatures of positive parity ($\pi = +$) Band 1 and negative parity ($\pi = -$) Band 2 in ^{194}Bi. For details on the data point in Band 2 connected by dashed line, see Sec. 4.2. Extracted i_x values for MR candidate Band 4 in ^{194}Bi are also shown. Values of $K = 9$, 7 and 8 are used for Bands 1, 2 and 4 in ^{194}Bi, respectively. For comparison, also i_x plots for low-lying strongly coupled rotational bands in neighbouring odd-A isotopes ^{193,195}Bi [2,3] and ^{193}Po [57] are shown. Please, note that in case of rotational bands in ^{193,195}Bi only band-head state configurations are given. The same Harris parameters as in [2,3] were used

spin states in the ^{193}Pb core. Another option involves the $i_{13/2}$ proton in the configuration of the excited states.

Interpretation of the rotational bands and their evolution as a function of spin in terms of aligned angular momenta (i_x) and B($M1$)/B($E2$) ratios [55,56] is provided.

4.1 Positive-parity Band 1

Band 1 with $I^{\pi}_{b.h.} = (10^+)$ is found to be slightly non-yrast, despite the observation that it is the most strongly populated structure in ^{194}Bi. This feature of Band 1 is graphically illustrated in Fig. 5, which visualises the energy of the states minus a rigid-rotor reference term, $E_{rigidref} = aI(I+1)$ with $a = 0.007 MeV/\hbar^2$, to magnify the energy differences between the states of the same spin, particularly the energy levels of Bands 1 and 2. It may suggest that there should be one low-energy transition below the 142 keV transition in the positive-parity Band 1 (see Fig. 1). We found no evidence for such a transition in the data.

A configuration where $i_{13/2}$ neutron hole state couples to the odd proton occupying the deformed $13/2^+[606]$ Nilsson orbital, which originates from the $1i_{13/2}$ orbital, with a total $K = 9$, is attributed to the isomeric (10^+) band head. The high K value indicates that spins higher than allowed I_{max} can be explained as being generated by the strong coupling of the actual $p - n$ spin vector to the rotating oblate Pb core. A smoothly increasing trend of $E2$-transition energies, which is typical for regular rotational structures, is observed up to the topmost transition in Band 1.

Such a configuration assignment to Band 1 is supported by the following facts:

(i) In Fig. 6, the extracted aligned angular momenta of the (π,α) = (+,0) and (+,1) configurations in ^{194}Bi Band 1 match with the i_x values of the $\nu i^{-1}_{13/2}$ band in ^{193}Po. The obtained aligned angular momentum of $\sim 5\hbar$ is about one half of the alignment gain due to the pair of $i_{13/2}$ neutrons in ^{193,195}Bi.

(ii) Assuming the proposed configuration and moderate oblate deformation β = -0.18, experimental B($M1$)/B($E2$) ratios agree well with a theoretical estimate using a cranking approximation [see Fig. 7a].

(iii) In the TRS calculations for ^{193}Bi and ^{191}Bi, the positive-parity minima associated with the high-K $13/2^+[606]$ structure are located close to the oblate γ = -60° axis at $\beta \approx$ -0.21 [4]. This is again in a good agreement with our observation.

Experimentally measured reduced transition strengths B($E1$, 633 keV) $\approx 6.9\times10^{-7}$ W.u. and B($E1$, 529 keV) $\approx 1.8\times10^{-7}$ W.u. are weaker compared to typical hindrance of $\sim 10^{-5}$ - 10^{-6} for $E1$ transition in this mass region. In the case of the $(10^+) \rightarrow (10^-)$ transition, an order of magnitude more suppression can be caused by an orbital change from an oblate intruder $\pi i_{13/2} 13/2[606]$ to a spherical shell model $\pi h_{9/2}$. We find similar values of B($E1$) corresponding to the same orbital change in literature: 1.28×10^{-6} W.u. for the $13/2^+ \rightarrow 11/2^-$ 55 keV transition in ^{195}Bi [3];

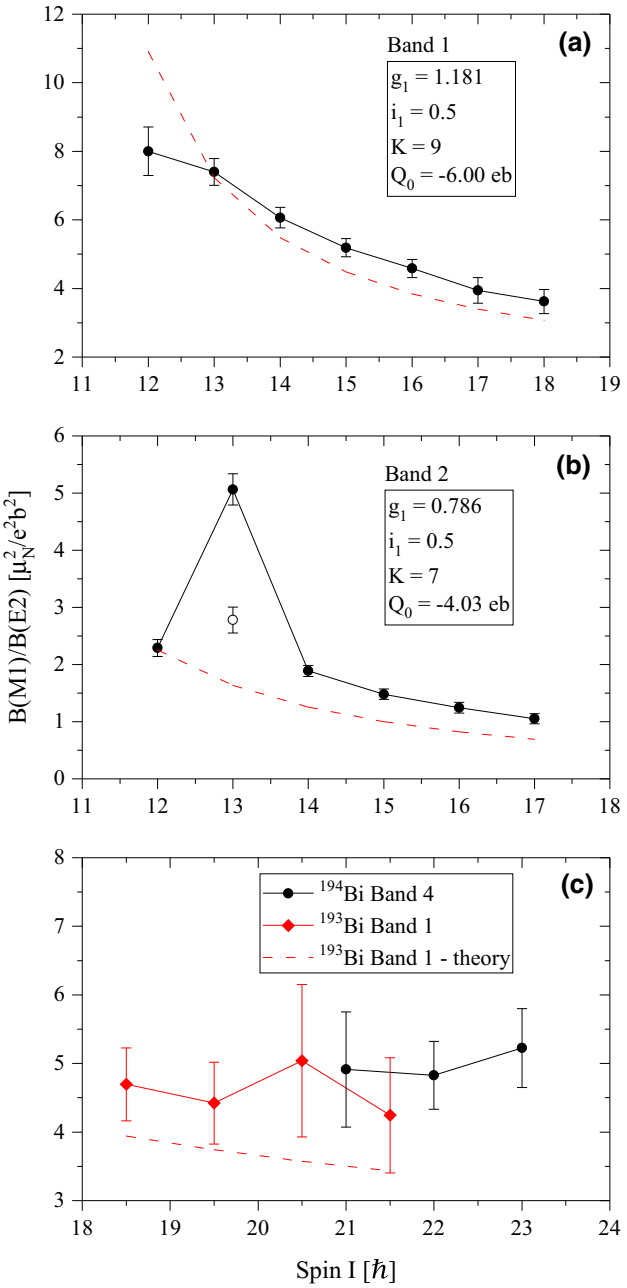

Fig. 7 (Colour online) Experimental B($M1$)/B($E2$) ratios for (a) Band 1, (b) Band 2, and (c) Band 4. For details on the data point denoted by empty circle in Band 2 , see Sec. 4.2. Also theoretical estimates [55,56] are shown as dashed red lines. On panel (c) are compared the experimental B($M1$)/B($E2$) ratios for Band 4 in ^{194}Bi to those for Band 1 in ^{193}Bi above the band crossing. Experimental values together with parameters needed for theoretical estimates for Band 1 in ^{193}Bi are taken from Ref. [2]

$2.2(9)\times10^{-6}$ W.u. for the $13/2^+ \rightarrow 11/2^-$ 59 keV transition and $6.2(13)\times10^{-7}$ W.u. for the $13/2^+ \rightarrow 13/2^-$ 114 keV transition in ^{201}At [16,17,58]. When compared to reduced transition strengths ($\sim10^{-8}$ W.u.) for the $11^- \rightarrow 10^+$ transitions in ^{188,190,194,196}Pb [59,60], a stronger hindrance in lead can be explained by the change from an oblate two-quasiproton configuration to a prolate two-quasineutron configuration.

4.2 Negative-parity Band 2

This collective structure is assigned a two quasiparticle configuration, having the $\nu i^{-1}_{13/2}$ coupled to the lowest negative-parity proton orbital at the oblate shape. The odd proton in the Band 2 configuration occupies either the $9/2^-[505]$ Nilsson orbital of $1h_{9/2}$ origin or $7/2^-[514]$ Nilsson orbital of mixed $f_{7/2}/h_{9/2}$ origin. Since the TRS calculations predict lower oblate deformation for the negative-parity configuration than for the positive-parity configuration in ^{193}Bi [4], Band 2 in ^{194}Bi is also expected to be less deformed than Band 1. This is consistent with the observed level patterns.

There is a sudden increase in aligned angular momentum in the beginning of the $\alpha = 1$ sequence of Band 2 (see Fig. 6). At the same time, the measured value of B($M1$)/B($E2$) ratio at a spin of $I = 13\hbar$ in Fig. 7b is rather off, even though the overall agreement with theoretical estimate is reached. This can be, at least partially, explained by the presence of the second (11^-) state located close to the (11^-) yrast state.

In our level scheme, two transitions, namely the 438 keV $(13^-) \rightarrow (11^-)$ $E2$ and the 108 keV $(12^-) \rightarrow (11^-)$ $M1$, feed the 911 keV level. Such a branching is a sign of mixing between the close-lying (11^-) states. The ratios of reduced transition strengths: $\frac{B(E2,438keV)}{B(E2,662keV)} \approx 1.8$, and $\frac{B(M1,108keV)}{B(M1,331keV)} \approx 3.6$ indicate that the level at 911 keV can be considered as a member of Band 2. Hence, level at 687 keV belongs to another level structure, *e.g.* Group B. In line with the above made conclusions, we add the new data points corresponding to two aforementioned transitions to both Figs. 6 and 7 (data points connected by dashed lines). We now see similar trend in i_x values between Band 2 and $\pi h_{9/2}$ band in ^{193}Bi [2], with $\sim 6\hbar$ gain in the alignment. This proves involvement of one $i_{13/2}$ neutron quasiparticle in the configuration of Band 2, as contribution from the high-K $h_{9/2}$ 9/2[505] proton to the i_x can be neglected.

4.3 Dipole bands

In light Bi nuclei, protons in the high-K $i_{13/2}$ and $h_{9/2}$ orbitals are known to play an important role in formation of nuclear structures at high excitation energy. This usually happens via their coupling to multi-quasiparticle structures in the Pb core, such as Pb_{8^+} and Pb_{11^-}. Holes in the partly filled $i_{13/2}$ neutron subshell contribute to the neutron spin. Small K values of such levels mean that a small component of the neutron angular momentum is projected onto the symmetry axis. A total spin of states near the band head is then characterised by coupling of the total j^π and j^ν spin vectors, which are nearly perpendicular. In ^{193}Pb, the isotone of ^{194}Bi, marking

the lower borderline of the region of regular magnetic rotation bands in the heavy Pb isotopes, negative parity neutron orbitals ($p_{3/2}$ and $f_{5/2}$) are involved in the configurations proposed for a dipole band [61].

Our configuration assignments for the proposed dipole bands in ^{194}Bi are suggested primarily on the basis of the comparison to our observations in the odd-A Bi isotopes.

In case of Band 3, electromagnetic character of the linking transitions dictates the lowest observed state to have a spin and parity of $I^{\pi} = (16^{+})$. In the ^{193,195}Bi nuclei, the $29/2^{+}$ isomeric states have been observed and explained as an $h_{9/2}$ proton coupled to $\pi(h_{9/2}i_{13/2})$ state in the Pb core. Owing to excitation energies of the $29/2^{+}$ isomeric states in the odd-A neighbours, 2350 keV and 2616 keV in ^{193}Bi and ^{195}Bi [2,3], respectively, and the band-head state in Band 3, we assign the $\pi(h^2_{9/2}i_{13/2}) \otimes \nu^{+}$ 4-qp configuration to dipole Band 3. Nevertheless, an option where $\pi h_{9/2} \otimes \nu i^{-2}_{13/2}$ couples to ν^{-} is equally possible. Assuming a positive parity for Band 5, both aforementioned configurations are also applicable to this band.

Similar transition energies between Band 4 and the positive-parity Band 1 in the odd-A Bi after 2-neutron alignments [2,3] lead to conclusion that the configuration of Band 4 might be $\pi i_{13/2} \otimes \nu i^{-2}_{13/2}$ coupled to negative-parity neutron in the $p_{3/2}$ orbital. For such a configuration, band-head spin is estimated to be $\sim (16\,\hbar)$. This estimate is obtained by adding the $I \approx 29/2\,\hbar$ of the lowest state for the $\pi i_{13/2}\nu i^{-2}_{13/2}$ configuration in ^{193}Bi [2] to the $I = 3/2\,\hbar$ for the neutron $p_{3/2}$ orbital. Levels of Band 4 are left without parity assignment, because no transition linking Band 4 with the lower-lying structures is observed. In this scenario, the two $i_{13/2}$ neutrons couple to zero K, and the final K value would have contribution of 6.5 from $\pi i_{13/2}$ and $\sim$ 1.5 from negative parity neutron, thus equal to 8. Experimental values of the aligned angular momenta for Band 4 are shown in Fig.6. Quantitatively, experimental $B(M1)/B(E2)$ ratios for Band 4 in ^{194}Bi and strongly coupled Band 1 in ^{193}Bi are comparable, as can be seen in Fig. 7. Band 4 can therefore be interpreted as a strongly coupled rotational band. A sudden drop of transition energies above $I = (25)$ in Band 4 may indicate a band crossing.

In order to make a reasonable systematics of dipole bands in the very neutron-deficient Bi isotopes, similar to that for Pb isotopes, more experimental data are needed.

4.4 Non-collective states

The two-quasiparticle plus rotor model [62] and the proton-particle neutron-quasiparticle quadrupole vibrator model [63] were successfully used to predict level crossings within the $\pi h_{9/2} \otimes \nu i^{-1}_{13/2}$ bands in ^{186,188}Tl [64]. In the $N = 111$ isotone, ^{192}Tl, the level crossing is not present anymore [29], and the 8^{-} state becomes the lowest state of the $I^{\pi} = 8^{-} - 10^{-}$ multiplet. In Ref. [29], an experimental evidence was given that the actual borderline nucleus for the level crossing in the multiplet in the very neutron-deficient odd–odd Tl isotope chain is ^{190}Tl, and not ^{188}Tl predicted by theory.

The same model [63] was applied on the neutron deficient odd–odd Bi isotopes, assuming the $p-n$ multiplet is coupled with the spherical Pb core, instead of an oblate deformed Hg core (odd–odd Tl). As a result, the (10^{-}) state was predicted to be the lowest state in the odd–odd Bi isotopes. Supporting evidence has been reported for odd–odd Bi isotopes down to ^{188}Bi [65]. Now, we provide the new evidence by marking the observation of the (9^{-}) state located 266 keV above the long-lived (10^{-}) isomeric state in ^{194}Bi. Moreover, the (11^{-}) state at 687 keV in our level scheme (see Fig. 1) is a candidate for the highest spin member of this multiplet. In ^{188}Bi, the $I^{\pi} = (9^{-},10^{-})$ state at 165 keV above the (10^{-}) isomeric state is considered to have its origin in a different $p-n$ multiplet $|\pi f_{7/2} \otimes \nu i^{-1}_{13/2}; J\rangle$ [65].

The (12^{-}) state at 1226 keV in Fig. 1, and level structure on top of it can be compared to observations for Group F in ^{193}Bi [2]. There, the $13/2^{-}$ state at 1067 keV above the $9/2^{-}$ ground state was interpreted as a single $h_{9/2}$ proton coupled to a spherical $Pb_{2^{+}}$-core state. In the ^{195}Bi nucleus, a similar $13/2^{-}$ state was also observed, only at higher excitation energy of 1199 keV [3]. In ^{194}Bi, we assume a configuration with a $\pi h_{9/2} \otimes \nu i^{-1}_{13/2}$ coupled to a spherical $^{192}Pb_{2^{+}}$-core state.

The energetically lowest-lying levels in Group A locate at excitation energies expected for the spherical $\pi i_{13/2} \otimes \nu i^{-1}_{13/2}$ configuration. In ^{193}Bi, the spherical $13/2^{+}$ state was found to be at 511 keV above the deformed $13/2^{+}$ [2].

5 Conclusion

Excited states above the long-lived (10^{-}) isomeric state in the odd–odd ^{194}Bi nucleus were studied by means of γ-ray spectroscopy. Nuclei of interest were produced in the ^{159}Tb(^{40}Ar,5n) fusion-evaporation reactions at JYFL, Finland. Low-lying strongly coupled rotational bands associated with the $\pi i_{13/2} \otimes \nu i^{-1}_{13/2}$ and $\pi h_{9/2} \otimes \nu^{-1}_{13/2}$ configurations were observed. Oblate deformation is assigned to both collective structures. A positive-parity band is built upon the (10^{+}) isomeric state with $T_{1/2} \approx 1$ ns. The main decay out of the band proceeds via a slightly hindered 633 keV $\Delta I = 0$ $E1$ transition. In the negative-parity band, an alternative decay path showing enhanced collectivity was found. Altogether three bandlike structures mainly composed of $\Delta I = 1$ $M1$ transitions have been observed in ^{194}Bi. A link to the oblate deformed, positive-parity band was established for one of the bands. Shears band character is attributed to this band. The

other two bands remain floating in our study. The band-head state of one of these bands is likely to be a short-lived isomer. Measured $B(M1)/B(E2)$ ratios excluded a shears band character for the second floating band. Observed features indicate a character of the strongly coupled rotational band. $B(M1)$ values for observed dipole bands need to be measured in order to unambiguously confirm their configuration assignments and shears band character.

Acknowledgements We would like to thank the personnel at the Accelerator Laboratory of the University of Jyväskylä. AH would like to thank the Slovak Research and Development Agency under contract No. APVV-15-0225, Slovak grant agency VEGA (contract No. 2/0129/17), and the project ITMS code 26210120023, supported by the Research and Development Operational Programme funded by ERDF (30%). Fruitful discussions with John L. Wood are much appreciated. This work was also supported by the United Kingdom Science and Technology Facilities Council (STFC) and by the Academy of Finland under the Finnish CoE Programme. The authors would like to thank the GAMMAPOOL European Spectroscopy Resource for the loan of germanium detectors for JUROGAM II.

Data Availability Statement This manuscript has associated data in a data repository. [Authors' comment: At present, the data are located on the disk storage, which is not available to public.]

References

1. A.K. Jain et al., Rev. Mod. Phys. **70**(3), 843 (1998)
2. A. Herzáň et al., Phys. Rev. C **92**, 044310 (2015)
3. A. Herzáň et al., Phys. Rev. C **96**, 014301 (2017)
4. P. Nieminen et al., Phys. Rev. C **69**, 064326 (2004)
5. B. Fant et al., J. Phys. G **17**, 319 (1991)
6. R.M. Clark et al., Phys. Lett. B **275**, 247 (1992)
7. G. Baldsiefen et al., Phys. Lett. B **275**, 252 (1992)
8. A. Kuhnert et al., Phys. Rev. C **46**, 133 (1992)
9. S. Frauendorf, Nucl. Phys. A **557**, 259c (1993)
10. A.O. Macchiavelli et al., Phys. Lett. B **450**, 1 (1999)
11. A. Gadea et al., Phys. Rev. C **55**, R1(R) (1997)
12. R.M. Clark et al., Phys. Rev. Lett. **82**, 3220 (1999)
13. F. Brandolini et al., Phys. Lett. B **388**, 468 (1996)
14. S. Rajbanshi et al., Phys. Rev. C **94**, 044318 (2016)
15. R.M. Clark, A.O. Macchiavelli, Annu. Rev. Nucl. Part. Sci. **50**, 1 (2000)
16. K. Auranen et al., Phys. Rev. C **91**, 024324 (2015)
17. K. Auranen et al., Phys. Rev. C **97**, 024301 (2018)
18. J.R. Novak et al., Phys. Rev. C **59**, R2989(R) (1999)
19. D.J. Hartley et al., Phys. Rev. C **78**, 054319 (2008)
20. H. Pai et al., Phys. Rev. C **90**, 064314 (2014)
21. G.K. Mabala et al., Eur. Phys. J. A **25**, 49 (2005)
22. P.J. Dagnall et al., J. Phys. G: Nucl. Part. Phys. **20**, 1591 (1994)
23. W.P. Alford et al., Phys. Rev. C **3**, 860 (1971)
24. U. Hagemann et al., Nucl. Phys. A **197**, 111 (1972)
25. K. H. Kaun *et al.*, Joint Institute for Nuclear Research, Dubna, Report No. E6-6808, 1972
26. T. Lönnroth et al., Z. Phys. A **287**, 307 (1978)
27. T. Lönnroth et al., Phys. Scr. **23**, 774 (1981)
28. B.V. Thirumala et al., Nucl. Phys. A **362**, 71 (1981)
29. P. van Duppen, P. Decrock, P. Dendooven, M. Huyse, G. Reusen, J. Wauters, Nucl. Phys. A **529**, 268 (1991)
30. M. Huyse et al., Phys. Rev. C **46**, 1209 (1992)
31. S. S. Wang, The Methods of Particle and Nuclear Experiments (unpublished), p/ 268
32. J. Stanja et al., Phys. Rev. C **88**, 054304 (2013)
33. L. Ghys et al., Phys. Rev. C **100**, 054310 (2019)
34. R.M. Clark et al., Phys. Rev. C **53**, 117 (1996)
35. H. Xiaolong, Nucl. Data Sheets **108**, 1093 (2007)
36. X.H. Zhou et al., Phys. Rev. C **54**, 2948 (1996)
37. G. Zwartz et al., J. Phys. G: Nucl. Part. Phys. **26**, 849 (2000)
38. M.E. Leino et al., Nucl. Instrum. Methods. Phys. Res. B **99**, 653 (1995)
39. J. Sarén et al., Nucl. Instr. Meth. A **654**, 508 (2011)
40. R.D. Page et al., Nucl. Inst. Meth. B **204**, 634 (2003)
41. I.H. Lazarus et al., IEEE Trans. Nucl. Sci. **48**, 567 (2001)
42. P. Rahkila, Nucl. Instr. Meth. A **595**, 637 (2008)
43. D.C. Radford, Nucl. Instrum. Methods Phys. Res. A **361**, 297 (1995)
44. D.C. Radford, Nucl. Instrum. Methods Phys. Res. A **361**, 306 (1995)
45. K.H. Schmidt et al., Phys. Lett. B **168**, 39 (1986)
46. K.S. Krane, R.M. Steffen, R.M. Wheeler, Nucl. Data Tables **11**, 351 (1973)
47. [39] K. Starosta et al., Nucl. Instrum. Methods Phys. Res., Sect. A **423**, 16 (1999)
48. E. Gueorguieva et al., Nucl. Instr. Meth. A **474**, 132 (2001)
49. T. Kibedi et al., Nucl. Instrum. Methods Phys. Res. A **589**, 202 (2008)
50. M. Nyman et al., Eur. Phys. J. A **51**, 31 (2015)
51. T. Lönnroth et al., Phys. Rev. C **33**, 1641 (1986)
52. H. Pai et al., Phys. Rev. C **85**, 064317 (2012)
53. T. Roy et al., Eur. Phys. J. A **51**, 153 (2015)
54. T. Chapuran et al., Phys. Rev. C **33**, 130 (1986)
55. S. Frauendorf, Phys. Lett. B **100**, 219 (1981)
56. F. Dönau, Nucl. Phys. A **471**, 469 (1987)
57. K. Helariutta et al., Eur. Phys. J. A **6**, 289 (1999)
58. K. Dybdal et al., Phys. Rev. C **28**, 1171 (1983)
59. G.D. Dracoulis et al., Phys. Rev. C **60**, 014303 (1999)
60. G.D. Dracoulis et al., Phys. Rev. C **72**, 064319 (2005)
61. G. Baldsiefen et al., Phys. Rev. C **54**, 1106 (1996)
62. A.J. Kreiner, Z. Phys. A **288**, 373 (1978)
63. J. Van Maldeghem, K. Heyde, Fizika **22**, 233 (1990)
64. A.J. Kreiner et al., Phys. Rev. Lett. **47**, 1709 (1981)
65. A.N. Andreyev et al., Phys. Rev. C **73**, 024317 (2006)